JOURNAL OF COMPUTATIONAL PHYSICS 99, 183–189 (1992)

An Anti-spatial-aliasing Filter for Explicit Modeling and Imaging in Inhomogeneous Media

ALVIN K. BENSON

Department of Geology and Geophysics, Brigham Young University, Provo, Utah 84602

Received January 31, 1990; revised April 10, 1991

An explicit finite difference solution to the scalar wave equation in isotropic, inhomogeneous media is completed by filtering out non-physical contributions to the data. This digital, anti-spatial-aliasing filter and some associated limits on angular frequency are determined. The filter is a projection operator determined from a constrained least-squares fit and can be implemented in the computer algorithm at either of two places. Furthermore, the filter should be applicable to *any* explicit finite difference solution to the wave equation. Unlike a standard dip filter, this filter is computationally flexible, efficient, and necessary in inhomogeneous media with rapid lateral and vertical velocity changes.

INTRODUCTION

In a previous paper [1] the two-dimensional scalar wave equation in isotropic, inhomogeneous media

$$R_{xx} + R_{zz} - \frac{4}{v^2(x, z)} R_{tt} = 0 \tag{1}$$

was Fourier transformed from time to angular frequency ω, and a coordinate transformation to a retarded time frame was invoked yielding the scalar wave equation

$$Q_{xx} + \omega^2 SQ - \frac{4i\omega}{\bar{v}} Q_z + Q_{zz} = 0, \tag{2}$$

in a shifted coordinate system, where S is the slowness function given by

$$S = \frac{4}{v^2} - \frac{4}{\bar{v}^2}. \tag{3}$$

This is the wave equation typically considered for modeling and data processing applications in geophysics [2].

An explicit polynomial series solution for Eq. (2) was given by

$$\bar{Q}(x, z + \Delta z, \omega) = \sum_{m=0}^{M} C_m (\partial_{x^2} + \omega^2 S)^m (\Delta x)^{2m} Q(x, z, \omega) \tag{4}$$

in [1], and the depth differencing coefficients (c_m's) and lateral second-derivative coefficients were determined. A computer algorithm for imaging seismic data based upon the expression

$$R(x, z, 0) = \sum_{m, \omega} C'_m \left[\sum_k D(k) + \left(\frac{\bar{v}^2}{v^2} - 1 \right) \right]^m \times e^{-i\omega 2z/\bar{v}} R(x, o, \omega). \tag{5}$$

(x—2nd difference operator)

was developed. This expression needs to be altered in order to remove noise due to spatial aliasing.

FORMULATING THE PROBLEM

In paper [1] the lateral second-difference coefficients were determined over the acceptable values of the horizontal wavenumber, P. What are these values? There are two upper limits for P:

(a) For a given spatial sampling Δx, the Nyquist value of P will be

$$P_{\text{Nyq}} = \frac{\pi}{\Delta x}. \tag{6}$$

(b) Also, a dip angle α can be defined by $\sin \alpha \equiv Pv/2\omega$. Therefore, if $\alpha_{\max}$ is the maximum dip encountered, then P is also constrained by the equation

$$|P| \leqslant \frac{2\omega}{v} \sin(\alpha_{\max}), \tag{7}$$

0021-9991/92 $3.00

where v represents velocity and ω angular frequency. The minimum velocity in an area can be used for v in Eq. (2). Thus, the acceptable range of P is given by

$$|P| \leqslant \text{Min}\left(\frac{2\omega}{v}\sin(\alpha_{\max}), \pi/\Delta x\right). \tag{8}$$

Contributions to the data from anything greater than either of these values are nonphysical, spatially aliased values. They are sometimes referred to as evanescent values.

Notice in Eq. (4) that SQ appears to be a simple multiplication. However, while Eq. (7) limits the rate of change of the wavefield Q with x, SQ is not so limited. SQ can pick up contributions outside the limits set by Eq. (8), since there are numerous derivatives of SQ with respect to x in the operator $(\partial_x^2 + SQ)^m$ in Eq. (4). Consequently, high spatial frequency instabilities can be introduced into the system whenever

$$\frac{2\omega \sin(\alpha_{\max})}{v} < \frac{\pi}{\Delta x}. \tag{9}$$

This instability due to nonphysical numerical noise can be removed by applying an appropriate mathematical filter to the slowness function $S(x, z)$ *and/or* the output Q on the left-hand side of Eq. (4).

A Filtering Operator

One solution to this problem is to numerically estimate a projection operator which has the following properties:

$$\Lambda = \begin{cases} 1, & |P| < P_F \\ 0, & \text{otherwise,} \end{cases} \tag{10}$$

where P_F is a lateral wavenumber less than the Nyquist value. This will filter out the spatially aliased wavenumbers. We approximate Λ with a symmetric $2L+1$ length filter $\bar{A}$ given by

$$(\bar{A}Q)_j \equiv a_o Q_j + \sum_{l=1}^{L} a_l (Q_{j+l} + Q_{j-l}). \tag{11}$$

Trying a plane wave solution for Q in Eq. (11) yields

$$(\bar{A}Q)_j = \left(a_o + 2\sum_{l=1}^{L} a_l \cos(Pl\,\Delta x)\right) e^{iPx}. \tag{12}$$

Therefore, the set of projection operator coefficients, the a's, can be approximated by combining Eqs. (10) and (12) to yield

$$a_o + 2\sum_{l=1}^{L} a_l \cos(Pl\,\Delta x) = \begin{cases} 1, & |P| < \omega/v \sin(\alpha_{\max}) \\ 0, & \text{otherwise.} \end{cases} \tag{13}$$

The a's can be determined from Eq. (13) by minimizing the least-squares error between the left- and right-hand sides. Filters of this type have been designed for other applications. For example, see Bogner and Constantinides [3] and Phuc and Attikiouze [4].

Filter Coefficients

Generalizing, let us consider some function $f(P)$ (vs 1) in the top line of Eq. (10). The value of a_o is determined from the condition that the projector is 1 for $P = 0$, yielding

$$a_o = 1 - 2\sum_l a_l. \tag{14}$$

Placing the result in Eq. (14) into Eq. (13), the rest of the a's can then be determined in a least-squares sense by minimizing the functional E given by

$$\begin{aligned} E = \Bigg\{ & \int_{-P_F}^{P_F} \left| f(P) - \left\{1 + 2\sum_l [\cos(Pl\,\Delta x) - 1]\, a_l\right\}\right|^2 dP \\ & + \int_{-\pi/\Delta x}^{-P_F} \left| 0 - \left\{1 + 2\sum_l (\cos(Pl\,\Delta x) - 1)\right\} a_l \right|^2 dP \\ & + \int_{P_F}^{\pi/\Delta x} \left| 0 - \left\{1 + 2\sum_l (\cos(Pl\,\Delta x) - 1)\right\} a_l \right|^2 dP \Bigg\}. \end{aligned} \tag{15}$$

The resulting general equation for the a's is

$$\sum_l a_l \left(1 + \frac{\delta_{lj}}{2}\right) = \frac{\Delta x}{4\pi} \int_{-P_F}^{P_F} f(P)(\cos(Pj\,\Delta x) - 1)\, dP + \frac{1}{2}. \tag{16}$$

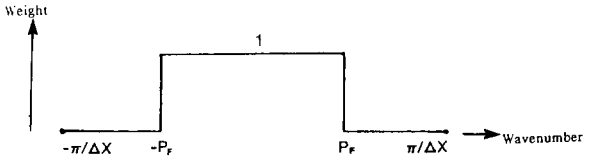

FIG. 1. A "box car" fit to determine the projection operator.

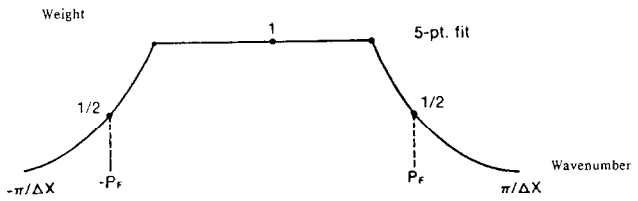

FIG. 2. A cosine-tapered fit to determine the projection operator.

If $f(P)=1$, the equation for evaluating the a's is

$$\sum_l a_l\left(1+\frac{\delta_{lj}}{2}\right)=\frac{1}{2}+\frac{\sin(jP_F\,\Delta x)}{2j\pi}-\frac{P_F\,\Delta x}{2\pi}. \tag{17}$$

A diagram representing the least squares fit for $f(P)=1$ is shown in Fig. 1. The a's can be generated numerically from Eq. (17) with a simple computer subroutine, taking l to be five or less.

In addition to Eq. (17), it has also been found that a five-point cosine-tapered fit produces a set of a's which gives very good results. A representation of this fit is shown in Fig. 2, where the value of the operator is chosen to be $\frac{1}{2}$ at $P=\pm P_F$. The Fourier transform of the a's is then given by

$$a_l=\sum_{k=-5}^{5}(a_k)\left(\frac{1}{11}\right)e^{-2\pi ilk/11}, \tag{18}$$

and the inverse Fourier transform by

$$a_k=\sum_{l=-5}^{5}a_l e^{i2\pi lk/11}, \tag{19}$$

where

$$a_k=\begin{cases}1 & k<P_F\\ \frac{1}{2} & k=P_F\\ 0 & k>P_F.\end{cases} \tag{20}$$

Combining Eqs. (18)–(20), the a_l's are

$$a_l=\frac{1}{11}\left[1+2\sum_{k=1}^{P_F-1}\cos\left(\frac{2\pi kl}{11}\right)+\cos\left(\frac{2\pi}{11}P_F l\right)\right]. \tag{21}$$

The a's generated from Eq. (17) or Eq. (21) can be used for the projection operator in Eq. (11) to filter out any non-physical spatial contributions to the solution in Eq. (4).

OTHER PROBLEMS

Some limits on the lateral wavenumber P were given in Eq. (8). Imposition of the projection (filter) operator also places a limit on P, which consequently, implies a minimum angular frequency allowed in the processed data. Let us determine this value.

Since the filter is basically represented by the sum

$$\sum_l a_l\cos(Pl\,\Delta x), \tag{22}$$

the first zero of this function occurs at

$$Pl\,\Delta x=\pi/2, \tag{23}$$

This means that the minimum value of P to produce zero is given by

$$P_{\min}=\frac{\pi}{2l\,\Delta x}. \tag{24}$$

But from Eq. (8) the desired zero is seen to be

$$P=\frac{\omega\sin\alpha}{v}. \tag{25}$$

Combining Eqs. (24) and (25) to solve for the minimum ω, we must have

$$\omega>\omega_{\min}\equiv\frac{v_{\min}\pi}{2l\,\Delta x\sin(\alpha_{\max})}. \tag{26}$$

This condition must be specified in the computer algorithm, and frequencies below this value not processed.

Another problem that can occur is instabilities at low frequencies. This can be significantly reduced by resampling the data more coarsely at low ω. Thus, for $P\,\Delta x<\pi/2$, the data can be resampled at every other point, for $P\,\Delta x<\pi/4$ at every fourth point, for $P\,\Delta x<\pi/8$ at every eighth point, etc. The skipped values can be put back into the final processed data using a $(\sin x)/x$ filter, or a linear interpolation of x values.

APPLICATION

The solution in Eq. (4) can be used to extrapolate recorded wavefields backwards in time through an estimated velocity structure. Imposition of an imaging condition, such as summing over the extrapolated frequencies, generates an image of the subsurface structure [5]. The migrated geophysical data are given by the explicit formula in Eq. (5), which is now altered to the form

$$R(x,z,0)=\sum_{m,\omega}C'_m\left[\sum_k D(k)+A\left(\frac{\bar{v}^2}{v^2}-1\right)\right]^m e^{-i\omega 2z/\bar{v}}R(x,o,\omega), \tag{27}$$

(x—2nd difference operator)

Migrated section; (z-differencing coefficients); (Projection operator); (Variable velocity $v(x,z)$); (Downward continuation operator); (Record section)

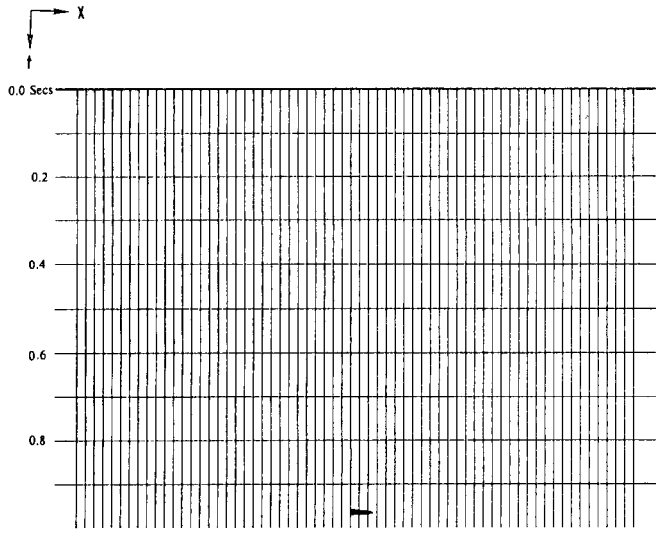

FIG. 3. Point diffractor in time.

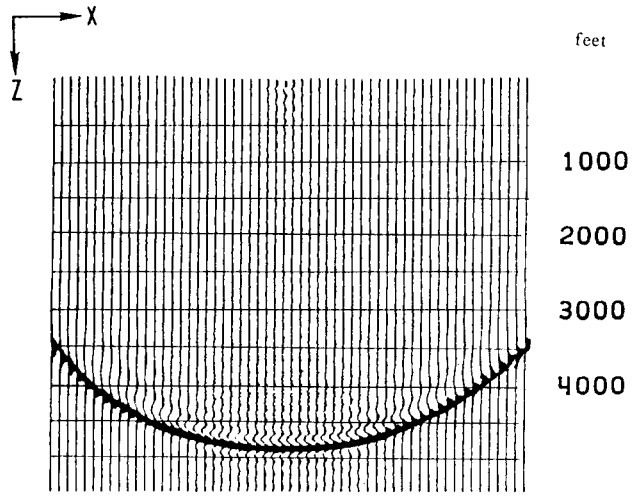

FIG. 5. Reconstructed hyperbolic reflector with projection operator applied.

where A is the projection operator developed in this paper. It is subject to the limits on the horizontal wave number in Eq. (8) and the associated limits on angular frequency in Eq. (26).

The migrated data $R(x, z, t=0)$ represent reflection coefficients at boundaries of velocity and/or density contrasts. This reflectivity function is obtained explicitly from the acquired surface data, $R(x, z=0, t)$, by the explicit operation in Eq. (27). The projection operator A removes spatially aliased data by filtering $S(x, z)$ as shown in Eq. (27), and/or it could also be applied to the reflectivity function $R(x, z+\Delta z, \omega)$ at each extrapolation step. The forward problem of modeling can also be formulated from the solution in Eq. (4) by changing all the signs in front of the depth z to the opposite sign.

As an example, let us consider a point diffractor in the subsurface. If this "source" were allowed to "explode" and send energy to the surface, a hyperbola would be recorded as a function of time [2]. This forward procedure is modeling. Collapsing the hyperbola back to a point at its true location is the task of migration. Similarly, if we consider a hyperbolic reflector "exploding" in the subsurface, it will generate a point amplitude as seen from the surface as a function of time. If the point is migrated, we should reproduce the hyperbolic reflector.

Figure 3 shows a point amplitude recorded in time at 0.964 s. Using the solution in Eq. (27) without applying the projection operator A, the point is extrapolated into the subsurface producing the hyperbola in Fig. 4. Notice the large amounts of spatially-aliased noise that are also generated. When the projection operator is included and applied to the slowness function in the polynomial solution, a much cleaner reflector is produced, as shown in Fig. 5.

Now let us consider the inhomogeneous case. A good question at this point would be why not use existing fan (dip) filter techniques? In order to minimize the spatial high frequency noise generated from the multiple derivatives in x

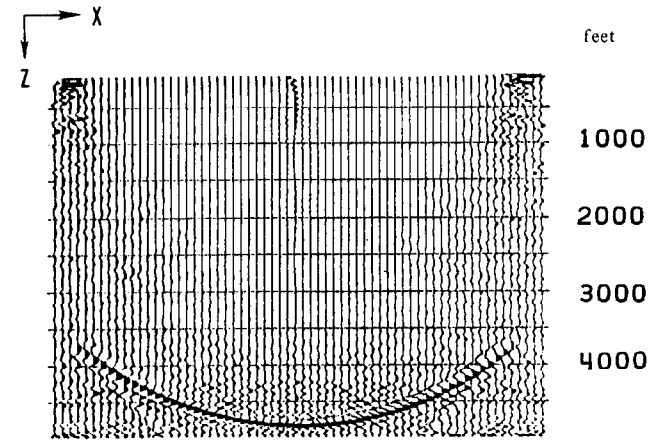

FIG. 4. Reconstructed hyperbolic reflector in depth with no projection operator applied.

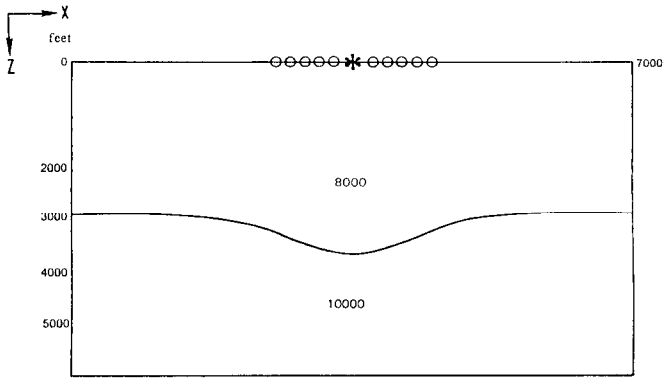

FIG. 6. Syncline depth model.

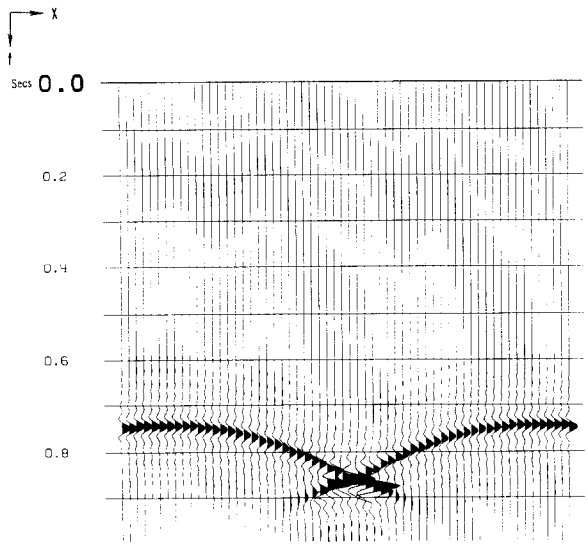

FIG. 7. Synthetic surface data from syncline model.

in Eq. (4), an appropriate filter must be applied at *each* extrapolation step and it must be a function of localized lateral velocity changes in any given area of the data. A standard f-k filter assumes homogeneous media, or at most, slowly varying velocity media. Hence, the anit-spatial-aliasing filter in Eq. (13) is much more flexible and computationally efficient for explicit depth imaging, and it is *necessary* to produce a superior image in inhomogeneous media with rapid vertical and lateral velocity changes.

As a inhomogeneous model, let us consider a classical syncline, as seen in Fig. 6. Vertical and lateral variations in velocity across the syncline are from 8000 to 10,000 ft/s. Spacing between traces is 110 feet, and the dip of the syncline flanks is about 14.5°. The known interval velocities shown in Fig. 6 are used to migrate the data.

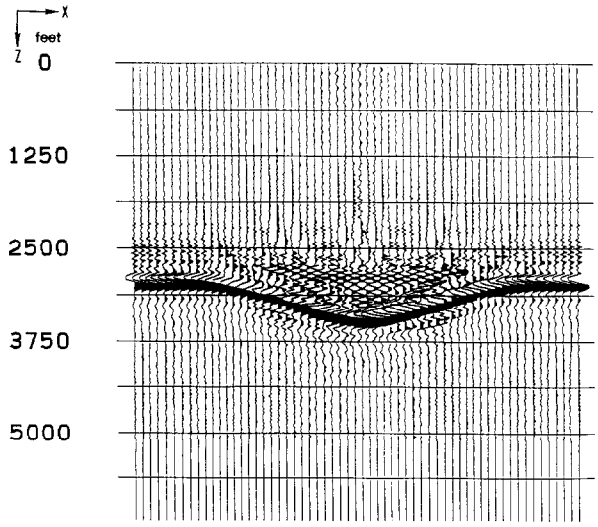

FIG. 8. Reconstructed syncline model without dip filtering or the anti-spatial-aliasing filter.

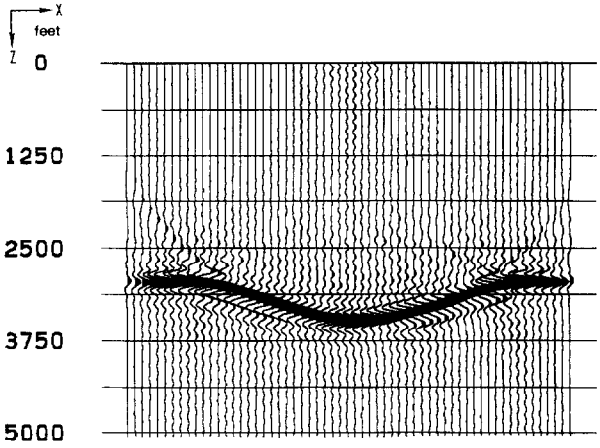

FIG. 9. Reconstructed syncline model using an algorithm based upon Eq. (27) with the anti-spatial-aliasing filter.

The modelled data in Fig. 7 were generated using a ray tracing algorithm. This represents synthetic surface seismic data acquired by setting off a source and recording the primary energy in receivers collocated with the source. It shows the characteristic "bow-tie" effect for a syncline. An attempted migration of this data without applying dip filtering or the anti-spatial-alising filter A is shown in Fig. 8. Large amounts of spatially-aliased noise are very evident. In contrast, imaging the simulated data with an algorithm based on Eq. (27), yields the depth cross section shown in Fig. 9. It is an excellent representation of the original model, except for some dispersion and some residual noise. As another comparison, a standard dip (fan) filter was applied to the data and the imaging was performed with the computer algorithm based on Eq. (5), without the anti-spatial-aliasing filter A. The results are shown in Fig. 10. The residual noise is much more prevalent, than in Fig. 9.

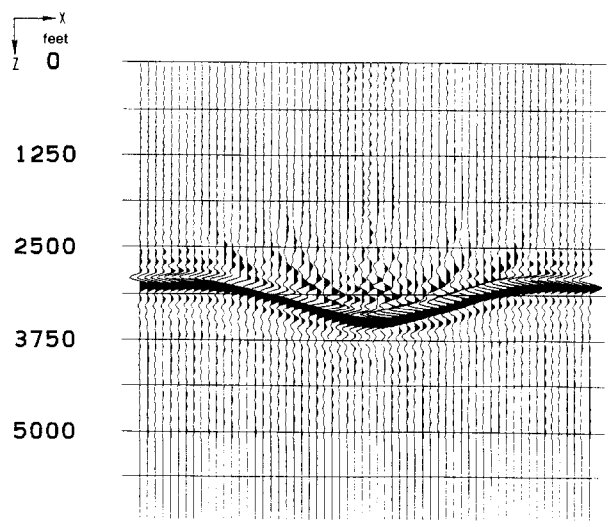

FIG. 10. Reconstructed syncline model using a standard dip (fan) filter vs the anti-spatial-aliasing filter.

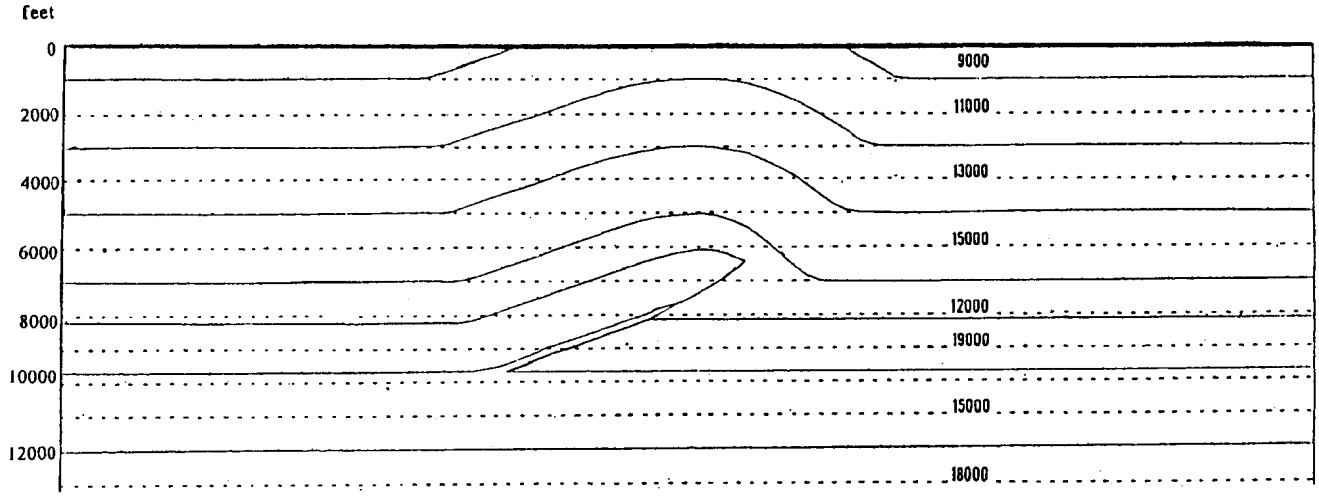

FIG. 11. Thrust fault model. Velocities are shown in feet per second.

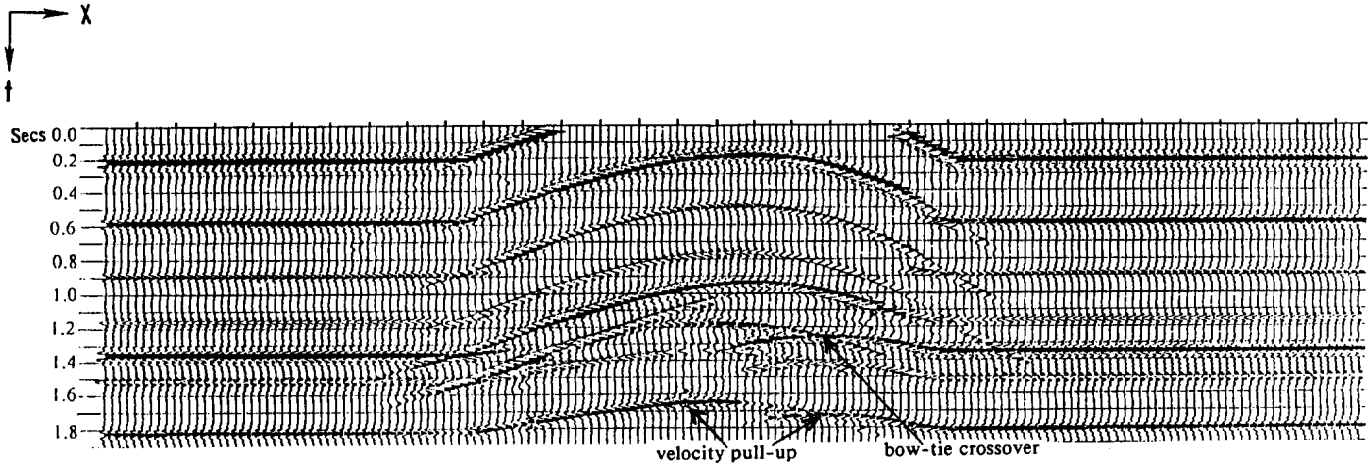

FIG. 12. Synthetic record section from the thrust fault model.

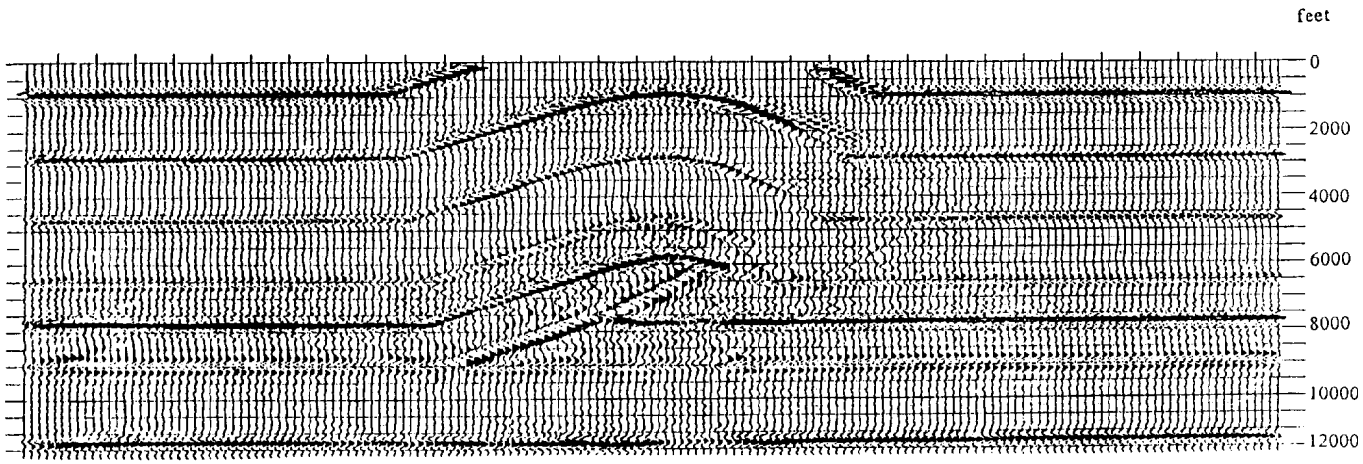

FIG. 13. Reconstructed thrust fault cross section using an algorithm based upon Eq. (27).

Clearly, the built-in anti-spatial-aliasing filter has done a superior job, as it has properly reduced spatially-generated noise associated with the multiple x-derivatives in Eq. (4) and the localized lateral velocity changes.

A complicated model of a thrust fault similar to those encountered in the Utah–Wyoming Overthrust Belt is shown in Fig. 11. A synthetic set of zero-offset surface data generated by ray tracing is shown in Fig. 12. It exhibits numerous bow-tie crossovers, velocity pull-up, and lower boundary undulations. It would be very difficult to interpret subsurface geology if only this data were used.

The depth imaged cross section obtained by feeding this simulated surface data and the interval velocities into an algorithm based upon Eq. (27) with the anti-spatial-aliasing filter A is shown in Fig. 13. It gives a very good overlay with the original subsurface model. The significant velocity pull-up in Fig. 12 has been correctly accounted for, and the lower boundary has been properly flattened. The depth image in Fig. 13 could be used for drilling decisions. For real data, a velocity model like that in Fig. 11 would have to be generated by self-consistent modeling [5].

The models in [1] were generated by truncating the frequency band to reduce spatial aliasing. The limits had to be considered and changed for every model at each depth step, depending on the velocities, dips, etc. involved, and this obviously changes as a function of position in general. The choice typically results in some loss of resolution, as well as extra decisions to make for every data set processed. It is computationally inefficient and very inflexible. However, the present digital filter automatically takes care of the problem in inhomogeneous media with maximum efficiency and/or migration resolution. Furthermore, this filter should be applicable to *any* explicit finite difference modeling scheme.

CONCLUSIONS

In this paper the algorithm developed in [1] has been altered by (a) filtering out spatially aliased values, with the filter coefficients given in Eq. (17) or (21), (b) limiting the lower frequency included in the processing according to Eq. (26), and (c) reducing low frequency instabilities by resampling the data spatially at low frequencies. Equation (27) is an explicit finite difference solution to the wave equation which can be used in many practical applications, such as generating synthetic surface data (modeling) and reconstructing subsurface horizons (migration). The solution works in inhomogeneous media where velocity changes rapidly both vertically and laterally, and the projection operator A, with associated frequency limits, filters out both inherent-data and numerically-generated spatially-aliased noise. As illustrated by some migration examples, a reconstructed image is obtained directly in depth with an excellent representation of the subsurface geology.

ACKNOWLEDGMENTS

The author extends appreciation to R. H. Stolt for many informative discussions.

REFERENCES

1. A. K. Benson, *J. Comput. Phys.* **87**, 47 (1990).
2. J. Claerbout, *Fundamentals of Geophysical Data Processing* (McGraw–Hill, New York, 1976).
3. R. E. Bogner and A. G. Constantinides (Eds.), *Introduction to Digital Filtering* (Wiley, New York, 1975).
4. D. T. Phuc and J. Attikiouzel, *Int. J. Electron.* **47**, 491 (1979).
5. R. H. Stolt and A. K. Benson, *Seismic Migration: Theory and Practice* (Geophysical Press, Amsterdam, The Netherlands, 1986).